Ocean Wave Directional Spectra Estimation from an HF Ocean Radar with a Single Antenna Array: Methodology

YUKIHARU HISAKI

Department of Physics and Earth Sciences, University of the Ryukyus, Nishihara-cho, Nakagami-gun, Okinawa, Japan

(Manuscript received 27 May 2004, in final form 10 April 2005)

ABSTRACT

A method to estimate ocean wave directional spectra using a high-frequency (HF) ocean radar was developed. The governing equations of wave spectra are integral equations of first- and second-order radar cross sections, the wave energy balance equation, and the continuity equation of surface winds. The parameterization of the source function is the same as that in WAM. Furthermore, the method uses the constraints that wave spectral values are smooth in both wave frequency and direction and that the propagation terms are small. The unknowns to be estimated are surface wind vectors at radial grids whose centers are the radar position, and wave spectral values at radial and wave frequency–direction grids. The governing equations are discretized in the radial and wave frequency–direction grids and are converted into a nonlinear minimization problem. Identical twin experiments showed that the present method can estimate wave spectra and dynamically extrapolate wave spectra, even in an inhomogeneous wave field.

1. Introduction

A directional spectrum is the most common way of describing the properties of ocean surface waves in energy (amplitude), frequency, and direction of propagation. Knowledge of ocean surface wave spectra is important in a wide variety of marine applications, such as physical oceanography, wave forecasting, ship routine, and coastal engineering. One promising method of measuring spatially evolving current and wave fields is to use high-frequency (HF) ocean radar, which measures ocean surface currents (e.g., Takeoka et al. 1995; Hisaki et al. 2001; Hisaki and Naruke 2003) and waves (Hisaki 1996, 2002, 2004) by radiating high-frequency radio waves and analyzing backscattered signals from the ocean. Since a Doppler spectrum can be expressed in terms of the wave directional spectrum, we can estimate that spectrum by inverting the integral equation that relates the Doppler spectrum to the wave spectrum (e.g., Wyatt 1990; Hisaki 1996; Hashimoto and Tokuda 1999; Hashimoto et al. 2003). These methods use dual-radar systems. However, there are obstacles to the use of HF ocean radars in measuring waves. One problem is that a wide area is necessary to deploy the HF radar's antenna. The coastal radar (CODAR)-type compact antenna systems (e.g., Lipa and Barrick 1986) require spatial homogeneity in the wave field over a wide area. It is difficult to obtain two wide radar sites near the shore. The other problem is that wave measurements by HF radar require a larger signal-to-noise level than current measurements, and hence the areas in which they are available are more likely to be restricted.

To overcome these problems, we developed a method to estimate wave directional spectra from an HF radar with a single antenna array. This method incorporates a wave model into the inversion method. The governing equations are the integral equation that relates the Doppler spectrum to wave spectra, the energy balance equation of waves under the assumption of stationarity, and the continuity equation of wind vectors under the assumption of no horizontal divergence. The radar changes its beam direction, and we can obtain Doppler spectra at radial grids on the polar coordinates whose center is the radar position. The energy balance equation and the continuity equation are expressed on the polar coordinates.

de Valk et al. (1999) attempted to estimate wave spectra from an HF ocean surface radar system by in-

Corresponding author address: Yukiharu Hisaki, Dept. of Physics and Earth Sciences, University of the Ryukyus, 1 Aza-Senbaru, Nishihara-cho, Nakagami-gun, Okinawa 903-0213, Japan.
E-mail: hisaki@sci.u-ryukyu.ac.jp

corporating the wave model into the inversion method. However, the wave energy input was not considered in their method. The present method considers wave energy inputs and also estimates sea surface winds. The integral equation describing the Doppler spectrum was linearized in their method, which requires spatial homogeneity in the short-wave field over a wide area. The present method does not linearize the integral equation.

The objective of the paper is to describe in detail a method for estimating ocean wave spectra from an HF radar with a single array using a data assimilation method. The present method for estimating wave spectra from HF radar is the first to fully incorporate the wave energy balance equation. The other objective of the paper is to verify the accuracy of the method by identical twin experiments. The only available data are the Doppler spectra observed by a single HF ocean radar.

Section 2 formulates the governing equations. These equations are expressed in discretized form in section 3. The method of numerical computation to estimate a wave spectrum is described in section 4. Section 5 describes the identical twin experiments to verify the accuracy of the wave estimation method. The results of the experiments are presented in section 6. The conclusions and future subjects are summarized in section 7. A comparison of estimated wave parameters with in situ measurements is the next subject of the study (Hisaki 2005).

2. Formulation

a. HF radio wave scattering from the sea surface

The main contribution to sea clutter is Bragg resonant scattering by surface gravity waves whose wavenumber vector is $\pm 2\tilde{\mathbf{k}}_0$, where $\tilde{\mathbf{k}}_0$ is the incident radio wavenumber vector [hereafter, a tilde ($\tilde{\ }$) denotes a dimensional variable]. A Doppler spectrum as a function of radian Doppler frequency $\tilde{\omega}_D$ shows two sharp peaks at the Bragg radian frequency

$$\tilde{\omega}_B = [2g\tilde{k}_0 \tanh(2\tilde{k}_0\tilde{d})]^{1/2}, \tag{1}$$

where g is the gravitational acceleration, $\tilde{d}$ is the water depth, and $\tilde{k}_0$ is the magnitude of $\tilde{\mathbf{k}}_0$, if there are no currents. These peaks, called first-order scattering, are surrounded by a continuum attributable to second-order effects, which is called second-order scattering. High-frequency radio wave scattering is based on the perturbation theory (Barrick 1971; Hisaki 1999; Hisaki and Tokuda 2001). Figure 1 shows a Doppler spectrum. We write quantities in the normalized form by the Bragg parameters as $\tilde{k}_0$ and $\tilde{\omega}_B$ (Lipa and Barrick

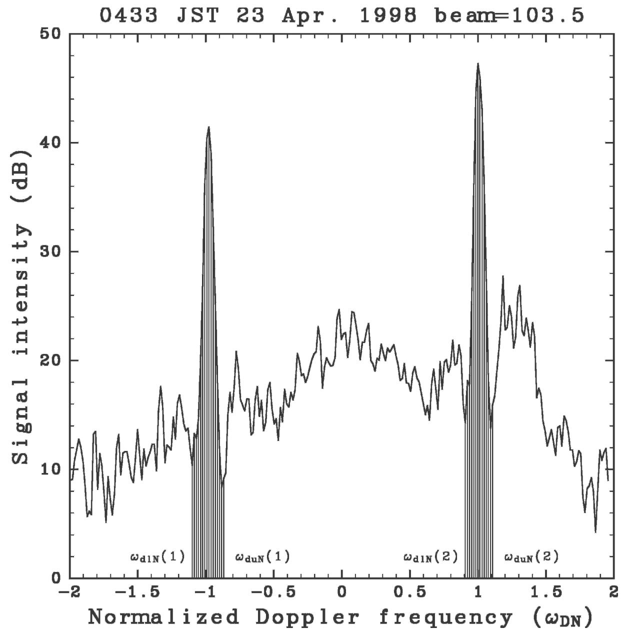

FIG. 1. An example of a Doppler spectrum $P(\omega_{DN})$. The shaded areas ω_{dlN} $(m) \le \omega_{DN} \le \omega_{duN}$ (m) $(m = 1, 2)$ denote first-order scattering regions for calculating Eq. (6).

1986). The subscript "N" denotes the normalized form by the Bragg parameters.

A Doppler spectral density $P(\omega_{DN})$ at a normalized Doppler frequency $\omega_{DN} = \tilde{\omega}_D/\tilde{\omega}_B$ is written in terms of a wave directional spectrum as

$$\left\{\int_0^\infty \sigma_{1N}[(2m-3)\omega_{DN}]\,d\omega_{DN}\right\}\left[\int_{-\infty}^\infty \sigma_{1N}(\omega_{DN})\,d\omega_{DN}\right]^{-1} = \int_0^\infty P_{c1}[(2m-3)\omega_{DN}]\,d\omega_{DN},\ (m = 1 \text{ or } 2) \tag{2}$$

and

$$\sigma_{2N}(\omega_{DN})\left[\int_{-\infty}^\infty \sigma_{1N}(\omega_{DN})\,d\omega_{DN}\right]^{-1} = P_{c2}(\omega_{DN}), \tag{3}$$

where

$$P_{ci}(\omega_{DN}) = P_i(\omega_{DN})\left[\int_{-\infty}^{+\infty} P_1(\omega_{DN})\,d\omega_{DN}\right]^{-1} \tag{4}$$

are the first- $(i = 1)$ and second-order $(i = 2)$ calibrated Doppler spectral densities, $P_1(\omega_{DN})$ and $P_2(\omega_{DN})$ are the first- and second-order Doppler spectral densities $[P(\omega_{DN}) = P_1(\omega_{DN}) + P_2(\omega_{DN})]$, and ψ_B is the beam direction. The calibration factor in Eq. (4) is estimated from a measured Doppler spectrum $P(\omega_{DN})$ as

$$\int_{-\infty}^{+\infty} P_1(\omega_{DN})\,d\omega_{DN} = \sum_{m=1}^{2} P_I(m), \tag{5}$$

$$P_I(m) = \int_0^\infty P_1[(2m-3)\omega_{\rm DN}]\, d\omega_{\rm DN}, \\ = \int_{\omega_{{\rm dl}N}(m)}^{\omega_{{\rm du}N}(m)} P(\omega_{\rm DN})\, d\omega_{\rm DN}, \qquad (6)$$

where $\omega_{{\rm dl}N}(m)$ and $\omega_{{\rm du}N}(m)$, respectively, are normalized lower and upper Doppler frequencies of the first-order scattering for the negative ($m = 1$) and positive ($m = 2$) Doppler frequency regions (Fig. 1).

The normalized integrated first-order radar cross section $[\sigma_{1N}(\omega_{\rm DN})]$ is written as

$$\int_0^\infty \sigma_{1N}[(2m-3)\omega_{\rm DN}]\, d\omega_{\rm DN} \\ = C_f G_N[1, \psi_B + (m-1)\pi], (m = 1, 2), \qquad (7)$$

where $G_N(\omega_N, \theta)$ is the normalized wave directional spectrum as a function of normalized wave frequency ω_N and wave direction θ, $\theta_b = \theta - \psi_B$ is the direction with respect to the beam direction, and the factor C_f is

$$C_f = 2\pi[1 + 2d_N \operatorname{cosech}(2d_N)] \qquad (8)$$

(Hisaki 1996). The factor C_f is derived by expressing Eq. (41) of Lipa and Barrick (1986) in terms of the wave spectrum $G_N(\omega_N, \theta)$. The normalized second-order radar cross section $[\sigma_{2N}(\omega_{\rm DN})]$ is written in Eq. (42) of Lipa and Barrick (1986) and Eq. (4) of Hisaki (1996). These equations show that the second-order radar cross section is related to the wave directional spectrum through the nonlinear integral equation.

The method to compute the second-order radar cross section $\sigma_{2N}(\omega_{\rm DN})$ numerically for a given Doppler frequency $\omega_{\rm DN}$ and a given wave spectrum $G_N(\omega_N, \theta)$ is described in sections 2.2 (deep water) and 2.3 (shallow water) of Lipa and Barrick (1986) and in section 2 of Hisaki (1996).

b. Wave energy balance

We assume the stationarity of wave fields. We also neglect the effect of the current on wave refraction. The energy balance equation is written as

$$\mathbf{C}_{gN} \cdot \nabla_N G_N(\omega_N, \theta) - S_{tN} = 0, \qquad (9)$$

where $\mathbf{C}_{gN} = \partial\omega_N/\partial k_N$ is the (normalized) group velocity vector of waves for wave frequency ω_N and wavenumber k_N, ∇_N denotes the horizontal gradient, and S_{tN} denotes the total wave energy input. The total energy source function S_{tN} is written as

$$S_{tN} = S_{{\rm in}N} + S_{{\rm ds}N} + S_{{\rm nl}N}, \qquad (10)$$

and the effect of bottom friction is neglected.

The parameterizations of $S_{{\rm in}N}$, $S_{{\rm ds}N}$, and $S_{{\rm nl}N}$ are almost the same as those in WAM cycle 3 (WAMDI Group 1988), because the derivatives of S_{tN} with respect to wave spectral values can be calculated from analytical equations. The wind input source function $S_{{\rm in}N}$ is adopted from Snyder et al. (1981). The relation is written in terms of the friction velocity u_{*N} and wind direction θ_w, and $S_{{\rm in}N}$ is written in the normalized forms of Eqs. (2.8) and (2.9) of the WAMDI Group (1988). The friction velocity u_{*N} is $u_* = C_D^{1/2} u_N$, where u_N is the normalized wind speed at 10-m height, and C_D is the drag coefficient, which is expressed in terms of a dimensional 10-m wind speed $\tilde{u} = u_N \tilde{\omega}_B (2\tilde{k}_0)^{-1}$ as $C_D = (0.8 + 0.065\tilde{u}) \times 10^{-3}$ [Eq. (11) of Wu (1980)].

The normalized dissipation source function $S_{{\rm ds}N}$ for deep water is adopted from Komen et al. (1984). The parameterization of $S_{{\rm ds}N}$ is slightly modified from that in Komen et al. (1984). The term $S_{{\rm ds}N}$ is written by Eqs. (2.14)–(2.18) of the WAMDI Group (1988), and it is written in terms of the normalized wave energy E_N and the parameter Ω_N, where

$$E_N = \int_{-\pi}^{\pi} \int_0^\infty G_N(\omega_N, \theta)\, d\omega_N\, d\theta \qquad (11)$$

and

$$\Omega_N = \int_{-\pi}^{\pi} \int_0^\infty G_N(\omega_N, \theta)\omega_N^{-1}\, d\omega_N\, d\theta. \qquad (12)$$

The nonlinear source function $S_{{\rm nl}N}$ is modeled using the discrete interaction approximation (DIA) (Hasselmann et al. 1985), which is an often-used approximation of the exact nonlinear transfer (Hasselmann 1962). In the DIA, two quadruplets with wavenumber vectors ($\mathbf{k}_{1N}$, $\mathbf{k}_{2N}$, $\mathbf{k}_{3N}$, $\mathbf{k}_{4N}$) satisfying the resonant condition [Eqs. (4.34) and (4.35) of Hasselmann (1962)], and with wave frequencies (ω_{1N}, ω_{2N}, ω_{3N}, ω_{4N}) satisfying Eqs. (5.1)–(5.3) of Hasselmann et al. (1985), are used to calculate nonlinear source function $S_{{\rm nl}N}$. The increments of wave energy due to the nonlinear interaction at wavenumber vectors $\mathbf{k}_{1N}(= \mathbf{k}_{2N})$, $\mathbf{k}_{3N}$, and $\mathbf{k}_{4N}$ are $\delta S_{{\rm nl}N}$, $\delta S_{{\rm nl}N}^{+}$, and $\delta S_{{\rm nl}N}^{-}$, which are written as the normalized form of Eq. (5.5) of Hasselmann et al. (1985).

The propagation term $\mathbf{C}_{gN} \cdot \nabla_N G_N(\omega_N, \theta)$ in Eq. (9) is written in the polar coordinates (r_N, ψ):

$$\mathbf{C}_{gN} \cdot \nabla_N G_N(\omega_N, \theta) = C_{{\rm gr}N} \frac{\partial G_N(\omega_N, \theta)}{\partial r_N} \\ + \frac{C_{g\psi N}}{r_N} \frac{\partial G_N(\omega_N, \theta)}{\partial \psi}, \qquad (13)$$

where C_{grN} and $C_{g\psi N}$ are the radial and azimuthal components of a group velocity vector. They are written as

$$(C_{grN}, C_{g\psi N}) = C_{gN}[\cos(\theta - \psi), \sin(\theta - \psi)]. \quad (14)$$

The source function S_{tN} determines the wave spectral shape. The nonlinear transfer function S_{nlN} of Eq. (9) is responsible for forming and maintaining the shape of the spectrum. This constraint is important, especially for those radial points at which second-order scattering is unavailable. Because the spectra at different positions are related by the propagation term, the spectrum at a radial point where the second-order scattering is unavailable is inferred from the constraint (9). The magnitudes of the three terms are dependent on the spectral shape. There are no terms whose magnitudes are much smaller than those of other source functions in all frequencies. Therefore, all three terms are important for the inversion, and none can be neglected in the source functions. The wind input term S_{inN} is expressed not only on the spectrum $G_N(\omega_N, \theta)$ but also on wind vector $\mathbf{u}_N$, so wind vector $\mathbf{u}_N$ should be estimated in the present method.

The continuity equation of the nondivergent sea surface wind vector $\mathbf{u}_N$ at 10-m height is written as

$$\boldsymbol{\nabla}_N \cdot \mathbf{u}_N = 0 \quad (15)$$

or

$$\cos(\theta_w - \psi)\left(\frac{\partial u_N}{\partial r_N} + \frac{u_N}{r_N}\frac{\partial \theta_w}{\partial \psi}\right) - \sin(\theta_w - \psi) \times \left(u_N \frac{\partial \theta_w}{\partial r_N} - \frac{1}{r_N}\frac{\partial u_N}{\partial \psi}\right) = 0. \quad (16)$$

The wind vectors are not necessarily the same at all grids. In fact, the observed ratios of first-order scattering differ from each other in one beam direction, which shows that wind direction varies along the beam direction. The constraint (15) allows horizontal variability of the estimated wind field. On the other hand, the constraint of the two-dimensional continuity equation acts as a regularization constraint in a polar grid. This constraint can be used to avoid the unrealistic spatial change of estimated wind vectors.

We estimate wave spectra $G_N(\omega_N, \theta)$ and sea surface wind vectors $\mathbf{u}_N$ from observed $P_1(\omega_{DN})$ and $P_2(\omega_{DN})$ using Eqs. (2), (3), (9), and (15).

3. Discretizing the governing equations

a. Expression of a wave spectrum

Wave spectra $G_N(\omega_N, \theta)$ and 10-m sea surface wind vectors $\mathbf{u}_N$ are estimated on radial grids at

$$r_N = r_N(i_r) = r_{\min N} + \Delta r_N(i_r - 1), i_r = 1, \ldots, N_r \quad (17)$$

and

$$\psi = \psi_B = \psi_B(j_b) = \psi_{B\min} + \Delta_{\psi B}(j_b - 1), \quad j_b = 1, \ldots, N_B, \quad (18)$$

where r_N is the normalized distance from the radar, ψ_B is the counterclockwise angle with respect to the eastward direction, N_r is the number of ranges per beam direction, $r_{\min N}$ is the normalized closest distance, Δr_N is the range resolution, N_B is the number of beam directions, and ($\psi_{B\min}$, $\Delta_{\psi B}$) are the parameters of the beam direction. The wave spectral values are estimated on the ω_N–θ plane at

$$\omega_N = \omega_N(k) = \omega_{\min N}\Delta_\omega^{k-1}, (k = 1, \ldots, M_f) \quad (19)$$

and

$$\theta = \theta(l) = -\pi + \Delta_\theta(l - 1), (l = 1, \ldots, M_d), \quad (20)$$

$$\Delta_\theta = \frac{2\pi}{M_d}, \quad (21)$$

where k is the wave frequency number, M_f is the number of frequencies, $\Delta_\omega > 1$ is the increment of the frequency, l is the wave direction number, and M_d is the number of directions.

The governing equations (2), (3), (9), and (15) are expressed in terms of $G_N[\omega_N(k), \theta(l), r_N(i_r), \psi_B(j_b)] = G_N(k, l, i_r, j_b)$ at position $[r_N(i_r), \psi_B(j_b)]$. A wave spectrum $G_N(\omega_N, \theta) = G_N(\omega_N, \theta, r_N, \psi_B)$ is expressed by $G_N(k, l, i_r, j_b)$.

Figure 2 is the wave frequency–wave direction (ω_N–θ) plane, which illustrates the discretization schematically. The integral to compute the second-order radar cross section $\sigma_{2N}(\omega_{DN})$ is conducted along the curve in

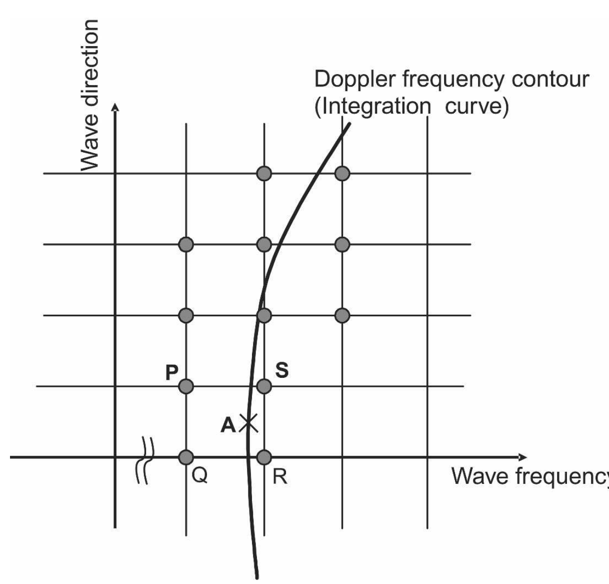

FIG. 2. Schematic illustration of the discretization by the spectral values on the wave frequency–direction (ω_N–θ) plane.

Fig. 2. For example, the spectral value at A in Fig. 2 is expressed by the spectral values at P, Q, R, and S, if the wave frequency ω_N at A in Fig. 2 is $\omega_{\min N} \le \omega_N \le \omega_{\max N}$, where $\omega_{\max N} = \omega_{\min N}\Delta_\omega^{M_f-1}$. The spectral value at A is extrapolated from the spectral values at P and Q according to the fourth inverse power of the wave frequency, if $\omega_N > \omega_{\max N}$ at A in Fig. 2. In the case of $\omega_N < \omega_{\min N}$, the spectral value at A in Fig. 2 is zero. Thus, the second-order radar cross section is expressed by the spectral values at grid points defined as Eqs. (19) and (20) in the ω_N–θ plane.

b. Discretizing the constraints

The second-order radar cross section at a Doppler frequency $\omega_{\mathrm{DN}} = \omega_{\mathrm{DN}}(m_D)$ and a position $[r_N(i_r), \psi_B(j_b)]$ is discretized by the spectral values in the four-dimensional $(\omega_N - \theta - r_N - \psi_B)$ space, where $m_D = 1, \ldots, K_D(i_r, j_b)$ is the Doppler frequency index number, and $K_D(i_r, j_b)$ is the number of Doppler spectral values at range number i_r and beam number j_b. The first-order radar cross section [Eq. (2)] is also discretized by the spectral values on the four-dimensional (ω_N–θ–r_N–ψ_B) space. Equation (9) is also discretized.

The propagation term $A_d(k, l, i_r, j_b)$, which is the first term in Eq. (9), contains spatial derivatives of wave spectra. The upwind scheme is used in the interior region. The boundary condition is not given here, and the forward or backward differentiation is used on the boundary. Values such as G_N and $\partial G_N/\partial r_N$ are not necessary on the boundary. Equation (13) is expressed in terms of $G_N[\omega_N(k), \theta(l), r_N(i_r), \psi_B(j_b)] = G_N(k, l, i_r, j_b)$ as

$$\begin{aligned} A_d(k, l, i_r, j_b) &= \mathbf{C}_{gN} \cdot \boldsymbol{\nabla}_N G_N(\omega_N, \theta) \\ &= C_{grN}(k, l, j_b)\frac{[G_N(k, l, i_r + m_{r1}, j_b) - G_N(k, l, i_r - m_{r2}, j_b)]}{(m_{r1} + m_{r2})\Delta r_N} \\ &\quad + \frac{C_{g\psi N}(k, l, j_b)}{r_N(i_r)}\frac{[G_N(k, l, i_r, j_b + m_{b1}) - G_N(k, l, i_r, j_b - m_{b2})]}{(m_{b1} + m_{b2})\Delta_{\psi B}}, \end{aligned} \tag{22}$$

where

$$(m_{r1}, m_{r2}) = (1, 0), \quad \text{for} \quad (i_r = 1) \quad \text{or} \quad (1 < i_r < N_r, C_{grN} \ge 0), \tag{23}$$

$$(m_{r1}, m_{r2}) = (0, 1), \quad \text{for} \quad (i_r = N_r) \quad \text{or} \quad (1 < i_r < N_r, C_{grN} < 0), \tag{24}$$

$$(m_{b1}, m_{b2}) = (1, 0), \quad \text{for} \quad (j_b = 1) \quad \text{or} \quad (1 < j_b < N_B, C_{g\psi N} \ge 0), \tag{25}$$

$$(m_{b1}, m_{b2}) = (0, 1), \quad \text{for} \quad (j_b = N_B) \quad \text{or} \quad (1 < j_b < N_B, C_{g\psi N} < 0). \tag{26}$$

The group velocity components $C_{grN}(k, l, j_b)$ and $C_{g\psi N}(k, l, j_b)$ are given by Eq. (14).

The source function $S_{tN} = S_{tN}(k, l, i_r, j_b)$, which is the second term in Eq. (9), is also discretized by the spectral values on the four-dimensional (ω_N–θ–r_N–ψ_B) space, wind speeds and directions on the polar (r_N–ψ_B) plane. The wind input term $S_{\mathrm{in}N} = S_{\mathrm{in}N}(\omega_N, \theta, r_N, \psi_B) = S_{\mathrm{in}N}(k, l, i_r, j_b)$ is written in terms of $G_N(k, l, i_r, j_b)$, $u_N = u_N(i_r, j_b)$, and $\theta_w = \theta_w(i_r, j_b)$ [Eqs. (2.8) and (2.9) of the WAMDI Group (1988) and Eq. (11) in Wu (1980)].

The wave energy E_N [Eq. (11)] and the parameter Ω_N [Eq. (12)] are discretized in terms of $G_N(k, l, i_r, j_b)$ by replacing the integral of Eqs. (11) and (12) to the weighted summation of spectral values. Thus, the dissipation term $S_{\mathrm{ds}N} = S_{\mathrm{ds}N}(\omega_N, \theta, r_N, \psi_B) = S_{\mathrm{ds}N}(k, l, i_r, j_b)$ is discretized by the spectral values on the four-dimensional space.

The source function $S_{\mathrm{nl}N}$ at $(\omega_N, \theta) = [\omega_N(k), \theta(l)]$ is written from the expressions of $\delta S_{\mathrm{nl}N}$, $\delta S^+_{\mathrm{nl}N}$ and $\delta S^-_{\mathrm{nl}N}$. The meanings of $\delta S_{\mathrm{nl}N}$, $\delta S^+_{\mathrm{nl}N}$, and $\delta S^-_{\mathrm{nl}N}$ were explained in section 2b. The source function $S_{\mathrm{nl}N}$ is the sum of $\delta S_{\mathrm{nl}N}$ for $\mathbf{k} = \mathbf{k}_{1N}$, $\delta S_{\mathrm{nl}N}$ for $\mathbf{k} = \mathbf{k}_{2N}$, $\delta S^+_{\mathrm{nl}N}$ for $\mathbf{k} = \mathbf{k}_{3N}$, and $\delta S^-_{\mathrm{nlN}}$ for $\mathbf{k} = \mathbf{k}_{4N}$, where $\mathbf{k}_N$ is the wavenumber vector for (ω_N, θ). In the case of $\mathbf{k}_N = \mathbf{k}_{3N}$, for example, wavenumber vectors $\mathbf{k}_{1N} = \mathbf{k}_{2N}$ and k_{4N}, and the wave frequencies $\omega_{1N} = \omega_{2N}$ and ω_{4N} are estimated from the resonant condition [Eqs. (4.34) and (4.35) of Hasselmann (1962) and Eqs. (5.1)–(5.3) of Hasselmann et al. (1985)]. The spectral values at wavenumber vectors $\mathbf{k}_{1N} = \mathbf{k}_{2N}$ and $\mathbf{k}_{4N}$ are evaluated by the spectral values on the ω_N–θ grid, as illustrated in Fig. 2. Thus, the increment $\delta S^+_{\mathrm{nl}N}$ can be expressed by the spectral values on the ω_N–θ grid from Eq. (5.5) of Hasselmann et al. (1985). The nonlinear source function $S_{\mathrm{nl}N} = S_{\mathrm{nl}N}(\omega_N, \theta, r_N, \psi_B) = S_{\mathrm{nl}N}(k, l, i_r, j_b)$ is also discretized by the spectral values in the four-dimensional (ω_N–θ–r_N–ψ_B) space. Equation (9) is discretized by the spectral values in the four-dimensional space and by wind speeds and directions on the polar (r_N–ψ_B) plane. The continuity equation of wind vectors [Eq. (15)] is discretized by centered differences in the interior region ($1 < i_r < N_r$, $1 < j_b < N_B$) and by the forward or backward differences on the boundary.

c. Regularization constraint

Wave spectral values should be smooth in the ω_N–θ plane. Therefore, in addition to the governing equations (2), (3), (9), and (15), the conditions at $[\omega_N(k), \theta(l)]$ as

$$\begin{aligned}\log[G_N(k+1, l)] + \log[G_N(k-1, l)] \\ + \log[G_N(k, l-1)] + \log[G_N(k, l+1)] \\ - 4\log[G_N(k, l)] = 0 \quad \text{for} \quad 1 < k < M_f\end{aligned} \tag{27}$$

or

$$\log[G_N(k, l-1)] + \log[G_N(k, l+1)] - 2\log[G_N(k, l)] = 0 \quad \text{for} \quad k = 1 \text{or} M_f. \tag{28}$$

Furthermore, the constraint as

$$\mathbf{C}_{\mathrm{gN}} \cdot \boldsymbol{\nabla}_N G_N(\omega_N, \theta) = 0 \tag{29}$$

is added to estimate wave spectra with a single radar. This constraint is not only for the small variation of wave spectral values in the polar plane but for reducing the underestimation of wave height in the case of dominant waves propagating perpendicular to the radar (e.g., Wyatt 2002). The addition of the constraint (29) does not significantly increase the computation time, because Eq. (29) is computed simultaneously with the computation of (9). On the basis of the discretization, the derivatives of all of the terms in the constraints (2), (3), (9), (15), (27), (28), and (29) with respect to unknowns (spectral values, wind speeds, and wind directions) are written in analytical form. The derivatives are numerically computed for the nonlinear minimization problem explained in section 4.

d. Discussion of the constraints

The assumptions of the present method are as follows. The perturbation theory of the HF radio wave scattering [Eqs. (2) and (3)] can be applied, and the wave height is not so high. Lipa and Barrick (1982) showed that the normalized significant wave height $H_{sN} = 4E_N^{1/2}$ should be smaller than 4.

The wave field and winds are almost stationary in time. The time scale for stationarity is the characteristic time scale of single scanning of the observation domain. Equation (9) implies that the winds and wave fields are not homogeneous throughout the HF radar observation area; that is the winds and spectra may be different in each radial grid. However, the winds and wave fields are homogeneous in each radar cell with radial resolution Δr_N and azimuthal resolution $\Delta\psi_B$. The parameterizations of the source function in the energy balance equation are approximated by those in WAM cycle 3 (WAMDI Group 1988). The WAM-3-type parameterization is adopted because of its simplicity. Computation time is important for practical use. The derivatives of the source function with respect to spectral values, wind speeds, or wind directions can be expressed in analytical form. If the parameterization of the source function is complicated, the derivatives of the source function with respect to spectral value or to the speeds or directions of wind are calculated by numerical differentiation. The computation time of the derivatives from their analytical form is shorter than that from numerical differentiation.

For example, DIA is adopted for the parameterization of nonlinear interactions. Recent studies showed that the directional distribution is bimodal at frequencies of approximately twice the peak frequency (e.g., Young et al. 1995; Ewans 1998; Hwang et al. 2000; Wang and Hwang 2001). The bimodal structure is maintained by the directional transfer of energy through nonlinear wave–wave interactions and is reproduced by the exact calculation (e.g., Banner and Young 1994; Young et al. 1995) of the nonlinear source function. If the bimodality of the directional distribution is true, it is difficult to estimate the bimodal distribution from HF radar. In order to estimate the bimodal distribution, S_{nlN} must be computed exactly. In addition, we cannot guarantee that it is possible to estimate the bimodal wave distributions with the use of many beam directions, even assuming the homogeneity of wave fields over a large area (Hisaki 2004).

The effect of the horizontal current shear on wave refraction is neglected [Eq. (9)]. If we consider the effect of the horizontal current shear, the wave energy balance equation [Eq. (9)] should be replaced with the wave action balance equation, and the dual-radar system should be used to estimate surface currents. The spatial change of spectral values is not so large. The change of spectral values in the wave frequency–wave direction plane is not so large.

The effects of winds on waves are integrated over long periods of time and over large distances far from the observation point. The waves near the spectral peak are insensitive to the local wind, so it is difficult to estimate wind speeds from Doppler spectra. A method to infer wind speeds is described in section 4c.

4. Inversion method

a. Unknowns and constraints

The number of unknowns N_u is

$$N_u = N_s + 2N_g, \tag{30}$$

$$N_g = N_r N_B, \tag{31}$$

$$N_s = M_f M_d N_g, \tag{32}$$

where N_g is the number of radial grid points, and N_s is the number of wave spectral values on all radial grids. The equations are wave energy balance equations, continuity equations, radar cross-section equations, and regularization constraints. The total number of equations is

$$N_t = M_t + 2N_s, \tag{33}$$

where

$$M_t = N_s + 2N_g + K_{\mathrm{DT}} = N_s + 2N_g + \sum_{i_r=1}^{N_r}\sum_{jb=1}^{N_B} K_D(i_r, j_b) \tag{34}$$

is the number of constraints of the radar cross-section equations, energy balance equations, and continuity equations. The number $K_D(i_r, j_b)$ is the number of Doppler spectral values at range number i_r and beam number j_b, and K_{DT} is the total number of second-order Doppler spectral values for wave estimation.

The governing equations (2), (3), (9), (15), (27), (28), and (29) are written in vector form as

$$\mathbf{F}(\mathrm{x}) = \mathbf{0}, \tag{35}$$

$$\mathbf{x} = (x_L), L = 1, \ldots, N_u, \tag{36}$$

$$\mathbf{F} = (F_K), K = 1, \ldots, N_t, \tag{37}$$

where $\mathbf{x}$ is unknown. A component of $\mathbf{x}$ denotes a wind speed, wind direction, or spectral value. The component x_L is $x_L = \log[G_N(k, l, i_r, j_b)]$ for $L \le N_s$, x_L $\log[u_N(i_r, j_b)]$ for $N_s < L \le N_g + N_s$, and $x_L = \theta_w(i_r, j_b)$ for $N_g + N_s < L \le N_u$. The vector function $\mathbf{F}$ represents the governing equations. The vector function $\mathbf{F}$ denotes the wave energy balance equation [Eq. (9)] for $1 \le K \le N_s$ and the continuity equation [Eq. (15)] for $N_s < K \le N_s + N_g$. The vector function $\mathbf{F}$ is the logarithmic form of the first-order radar cross-section equation [Eq. (2)] for $N_s + N_g < K \le N_s + 2N_g$, and the logarithmic form of the second-order radar cross-section equation [Eq. (3)] for $N_s + 2N_g < K \le M_t$. The function denotes a regularization constraint in the $\omega - \theta$ plane [Eq. (27) or (28)] for $M_t < K \le M_t + N_s$ and a regularization constraint in the polar plane [Eq. (29)] for $M_t + N_s < K \le N_t$.

The vector $\mathbf{x}$ is estimated by seeking the minimum of the objective function $U(\mathbf{x})$ defined as

$$U(\mathbf{x}) = U(\mathbf{x}, K_s, K_e) = \frac{1}{2}\sum_{K=K_s}^{K_e} [\lambda_{\mathrm{wM}} FK(\mathbf{x})]^2 = \frac{1}{2}\sum_{K=K_s}^{K_e} [f_K(\mathbf{x})]^2, \tag{38}$$

where $K_s = 1$, $K_e = N_t$, and $f_K = \lambda_{\mathrm{wM}} F_K$ ($K = 1, \ldots, N_t$). The parameter λ_{wM} ($M = 1, \ldots, 6$) is the weight, and $M = 1$ for $1 \le K \le N_s$ [energy balance equation (9)], $M = 2$ for $N_s < K \le N_s + N_g$ [continuity equation (15)], $M = 3$ for $N_s + N_g < K \le N_s + 2N_g$ [first-order radar cross-section equation (2)], $M = 4$ for $N_s + 2N_g < K \le M_t$ [second-order radar cross-section equation (3)], $M = 5$ for $M_t < K \le M_t + N_s$ {regularization constraint in the $\omega - \theta$ plane [(27) or (28)]}, and $M = 6$ for $M_t\, N_s < K \le N_t$ [regularization constraint in the polar plane (29)].

b. Algorithm for nonlinear optimization problem

The minimization of $U(\mathbf{x})$ is solved numerically, and the algorithm is expressed as

$$\mathbf{d}_m = -\mathbf{H}^{(m)}\nabla U = -\mathbf{H}^{(m)}\mathrm{J}_{\mathrm{f}}^{\mathrm{T}}\mathbf{f}, \tag{39}$$

$$\mathbf{x}^{(m+1)} = \mathbf{x}^{(m)} + \alpha_m \mathbf{d}_m, \tag{40}$$

where m indicates the step number, and α_m is a positive constant that has been adjusted such that $U(\mathbf{x}^{(m+1)}) < U(\mathbf{x}^{(m)})$. The vector $\mathbf{x}^{(m)} = (x_1^{(m)}, \ldots, x_{N_u}^{(m)})$ is $\mathbf{x}$ for the mth step. The vector $\mathbf{f} = (f_K) = (\lambda_{\mathrm{wM}} F_K)$ ($K = 1, \ldots, N_t$), and $\mathbf{J}_\mathbf{f}$ is the Jacobian matrix defined as

$$\mathbf{J}_\mathbf{f}(\mathbf{K},\mathbf{L}) = \frac{\partial f_K}{\partial x_L^{(m)}} \quad (K = 1, \ldots, N_t) \quad (L = 1, \ldots, N_u). \tag{41}$$

The $N_u \times N_u$ matrix $\mathbf{H}^{(m)}$ is positive definite. It is difficult to keep the $N_u \times N_u$ matrix in computer memory because it requires a huge amount of memory. This storage problem is avoided by choosing the matrix $\mathbf{H}^{(m)}$ as a diagonal matrix such as

$$\mathbf{H}^{(m)} = [\mathrm{diag}(\mathbf{J}_\mathrm{f}^{\mathrm{T}}\mathbf{J}_\mathrm{f})]^{-1} \tag{42}$$

or

$$\mathbf{H}^{(m)} = [\mathrm{diag}(\mathbf{J}_\mathrm{f}^{\mathrm{T}}\mathbf{J}_\mathrm{f}) + 1]^{-1}, \tag{43}$$

or $\mathbf{H}^{(m)} = \mathbf{I}$ (steepest descent method), where I is the unit matrix. The updating direction $\mathbf{d}_\mathrm{m} = (d_L)$ ($L = 1, \ldots, N_u$) is written as

$$d_L = \left[\sum_{K=1}^{M_t} f_K \frac{\partial f_K}{\partial x_L}\right]\left[\sum_{K=1}^{M_t}\left(\frac{\partial f_K}{\partial x_L}\right)^2\right]^{-1}, (L = 1, \ldots, N_u) \tag{44}$$

if Eq. (42) is adopted. The derivative $\partial f_K/\partial x_L = \lambda_{wM}\partial F_K/\partial x_L$, or $\partial F_K/\partial x_L$ is calculated from the analytical form of the derivative.

The updating vector $\mathbf{d}_m = (d_L)$ is directed to reduce $U(\mathbf{x})$; that is $U(\mathbf{x}^{(m+1)}) = U(\mathbf{x}^{(m)} + \alpha_m \mathrm{d}_m) \le U(\mathbf{x}^{(m)})$, if α_m (> 0) is sufficiently small in Eq. (39). This is because $\mathrm{H}^{(m)}$ is the positive definite matrix and because $\partial U(\mathrm{x}^{(m)} + \alpha_m \mathbf{d}_m)/\partial \alpha_m \le 0$ at $\alpha_m = 0$. The objective function $U(\mathbf{x})$ can be decreased in the algorithm [Eq. (39)] by selecting α_m properly. The optimal value of α_m is determined from a line search technique along the direction $\mathbf{d}_m$. However, it is necessary to evaluate $U(\mathbf{x})$ for various $\mathbf{x}$ in the line search technique, and this technique is not adopted because of its long computation time. An initial value of α_m is given, and if $U(\mathbf{x}^{(m+1)}) < U(\mathbf{x}^{(m)})$, the value of α_m is reduced. If α_m is too small to update $\mathbf{x}$ (i.e., $\alpha_m \simeq 0$ and $\mathbf{x}^{(m+1)} \simeq \mathbf{x}^{(m)}$), the form of the matrix $\mathrm{H}^{(m)}$ is changed, for example, from Eq. (42) to $\mathrm{H}^{(m)} = \mathrm{I}$. In case the decreasing ratio of $U(\mathbf{x})$ is small, the value of α_m is increased.

The maximum number of iterations of Eq. (40) is more than 100. In the examples presented here, the weighted mean difference of the radar cross section $\{(10 \log_{10} e)[2U(\mathbf{x}, N_s + N_g + 1, M_t)/(N_g + K_{\mathrm{DT}})]^{1/2}\}$ is less than 1 dB.

c. Initial guess

In estimating wave spectra and winds, the initial guess is important, not only because the convergence speed depends on it but also because the iteration scheme (39) does not seek the global minimum of $U(\mathbf{x})$ but rather the local minimum of $U(\mathbf{x})$. The initial wave spectra and winds are not dependent on radial grids (i_r, j_b). The initialization is divided into two steps.

The first step (step 1) is to estimate a wave spectrum in a parametric form. The wind direction is also estimated in the first step. To indicate a wave direction, a short-wave direction is better than a dominant wave direction.

The initial wind direction is estimated only from the first-order scattering. The short-wave directional distribution is proportional to $\cos^{2s}[(\theta - \theta_w)/2]$, and the parameters θ_w and s are estimated by seeking the minimum of $U(\mathbf{x}, N_s + N_g + 1, N_s + 2N_g)$ [Eq. (38)] using the Monte Carlo method. The relationships between first- and second-order Doppler spectra and wave spectra [Eqs. (2) and (3)] are used in step 1. The number of Monte Carlo trials is $M_c = 1024$.

The initial guess for wave spectra in step 1 is written as

$$\tilde{G}(\tilde{\omega},\theta) = \frac{G_N(\omega_N,\theta)}{\tilde{\omega}_B(2\tilde{k}_0)^2} = \tilde{\Psi}(\tilde{\omega})D(\tilde{\omega},\theta), \tag{45}$$

$$\tilde{\Psi}(\tilde{\omega}) = \alpha g^2 \tilde{\omega}^{-p} \exp\left[-\frac{p}{p-1}\left(\frac{\tilde{\omega}}{\tilde{\omega}_p}\right)^{1-p}\right], \tag{46}$$

$$D(\tilde{\omega},\theta) = D(\tilde{\omega}(k),\theta) = \cos^{2s}\left(\frac{\theta - \theta_a(k)}{2}\right) \times\left[\int_{-\pi}^{\pi} \cos^{2s}\left(\frac{\theta}{2}\right) d\theta\right]^{-1}, \tag{47}$$

where $\tilde{\Psi}(\tilde{\omega})$ is the frequency spectrum, $D(\tilde{\omega}, \theta)$ is the directional distribution, and $\theta_a(k)$ is the mean wave direction for frequency number k. The parameters α, $\tilde{w}_p$, p, s, and $\theta_a(k)$, ($k = 1, \ldots, M_f$) are estimated by seeking the minimum of $U(\mathbf{x}, N_s + N_g + 1, M_t)$ [Eq. (38)] using the Monte Carlo method. These parameters are randomly generated for decided parameter ranges, and $U(\mathbf{x}, N_s + N_g + 1, M_t)$ are estimated for these parameters. The parameters $\theta_a(k)$, ($k = 1, \ldots, M_f$) are chosen as

$$\theta_a(k) = \theta_w + (2r_k - 1)\Delta\theta_{\mathrm{bd}}, \quad \text{for} \quad k \ge k_B, \tag{48}$$

$$\theta_a(k) = \theta_a(k+1) + (2r_k - 1)\Delta\theta_{\mathrm{nd}}, \quad \text{for} \quad k < k_B, \tag{49}$$

where θ_w is the initial guess for wind direction, k_B is the frequency number as $\tilde{\omega}(k_B)$ is close to $\tilde{\omega}_B$, and r_k ($k = 1, \ldots, \mathrm{M}_f$) are the random numbers of $0 \le r_k \le 1$, $\Delta\theta_{\mathrm{bd}} = 15°$, and $\Delta\theta_{\mathrm{nd}} = 10°$.

The second step (step 2) is to estimate a wave spectrum by seeking the minimum of $U(\mathbf{x}) = U(\mathbf{x}, N_s + N_g, M_t + N_s)$. The relationships between first- and second-order Doppler spectra and wave spectra, and regularization constraints in frequency–direction grids are used in this step. Equations (2), (3), and (27) [or (28)] are used to estimate an initial spectrum in step 2. The scheme (39) is also used for each iteration. The $M_f M_d \times M_f M_d$ matrix $\mathbf{H}^{(m)}$ can also be computed as $\mathbf{H}^{(m)} = (\mathrm{J_f}^{\mathrm{T}}\mathrm{J_f} + \alpha_q{}^{\mathrm{I}})^{-1}$ $(0 \le \alpha_q \le 1)$ (the Levenberg–Marquardt method) in this case. To reduce computation time, the initial wave spectrum can be estimated from selected radial grids.

The initial wind speed is estimated from the initial equilibrium frequency spectrum. The equation (9) assumes that the equilibrium frequency spectrum depends on wind speeds. The wave spectra are estimated from Eq. (50) (but $C_{gxN}\partial G_N/\partial x_N = 0$, where C_{gxN} is the $\mathbf{x}$ component of the group velocity vector) for various wind speeds beforehand. The wind speed is inferred from an initial frequency spectral value at a high frequency by comparing spectra estimated from Eq. (50).

d. Summary of the method

In step 1, the wave spectra are assumed to be not dependent on grid points. The initial wave spectrum is expressed in a parametric form as Eqs. (45)–(49), and the wave spectrum is estimated from first- and second-order Doppler spectra using the Monte Carlo method, as explained in section 4c. The wind direction is estimated from the ratio of first-order scattering, as in the method described by Hisaki (2002).

The wave spectra are also assumed to be not dependent on grid points in step 2. The wave spectrum is discretized in the wave frequency–direction (ω_N–θ) plane. The spectral values are estimated from first- and second-order Doppler spectra, and smoothness constraints in the frequency–direction plane. The algorithm described in sections 4b and 4c is used to estimate the spectral values. The wind speed is estimated in step 2, as explained in section 4c.

In the final step, the wave spectra are dependent on grid points. The wave spectra are discretized in the wave frequency–direction–polar ($\omega - \theta - r - \phi$) space. All of the constraints described in sections 2 and 3c, including the relationships between first- and second-order Doppler spectra and wave spectra, wave energy balance equations, and regularization constraints, are used in the final step. The wave spectrum at the position where there is no second-order Doppler spectrum data is interpolated or extrapolated from the wave energy balance equation [Eq. (9)] and regularization constraints in polar grids [Eq. (29)]. The algorithm described in section 4b is used to estimate the spectral values.

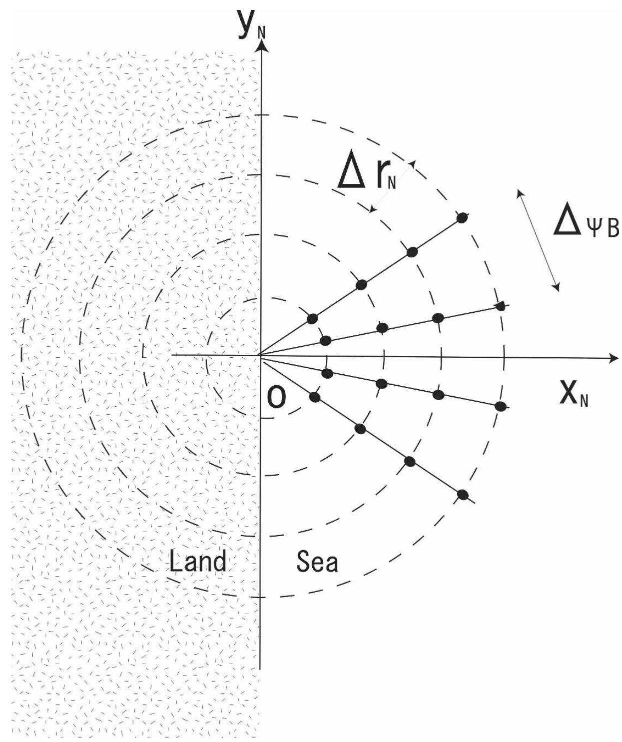

FIG. 3. Geometry of the radar position, the $\tilde{x} - \tilde{y}$ (or x_N–y_N) coordinates.

5. Twin experiments

Wave and radar parameters

To verify the accuracy of the method developed here, identical twin experiments are conducted. The identical twin experiments are described as follows. The wave spectra are simulated by integrating the wave energy balance equation in time for a given wind field. The Doppler spectra are simulated from simulated wave spectra. Then, the wave spectra and wind vectors are retrieved from simulated Doppler spectra.

The geometry of the radar position and the $\tilde{x} - \tilde{y}$ (or $x_N - y_N$) coordinates are shown in Fig. 3. For simplicity, the wave field is homogeneous in the $\tilde{y}$ direction, and a deep water case is considered. Wave spectra are simulated from the equation

$$\frac{\partial G_N}{\partial t_N} + C_{gxN}\frac{\partial G_N}{\partial x_N} - S_{tN} = 0, \tag{50}$$

where t_N is the normalized time, and the second and third terms are at the left-hand side of Eq. (9). The boundary condition is $G_N = 0$ at $\tilde{x} = 0$ ($x_N = 0$) and $\partial G_N/\partial x_N = 0$ at $\tilde{x} = x_L$. The boundary condition at $\tilde{x} = 0$ affects the wave spectra in the HF radar observation area, while the effect of the boundary condition at $\tilde{x} = x_L$ on the wave spectra in the HF radar observation area is negligible.

The parameters are as follows. The dimensional time step $\Delta\tilde{t} = 60$ s, the grid space $\Delta\tilde{x} = 3000$ m, $x_L = 3000$ km, the dimensional minimum frequency $\tilde{f}_{\min} = \omega_{\min N}\tilde{\omega}_B/(2\pi) = 0.0497$ Hz, the maximum frequency $\tilde{f}_{\max} = \omega_{\max N}\tilde{\omega}_B/(2\pi) = 0.813$ Hz, the frequency increment $\Delta_\omega = 1.15$, $M_f = 21$, and $M_d = 18$. The computation of Eq. (50) is the same as that in the WAMDI Group (1988): A semi-implicit scheme is adopted to integrate the source function, and the first-order upwind scheme is adopted to integrate advective terms. The wave growth limiter

$$\max(|\Delta G_N|) = 5 \times 10^{-4} C_{gN}^{-3} k_N^{-3} \tag{51}$$

was introduced (Tolman 1992). The integration time is 48 h in the examples presented here.

First- and second-order Doppler spectra are simulated as

$$P_I(m) = C_f G_N[1, \psi_B + (m-1)\pi]\chi^2(\nu_1)\nu_1^{-1}\ (m = 1, 2), \tag{52}$$

$$P_2(\omega_{DN}) = \sigma_{2N}(\omega_{DN})\chi^2(\upsilon_2)\upsilon_2^{-1}, \tag{53}$$

where $\chi^2(\upsilon_1)$ and $\chi^2(\upsilon_2)$ are χ-squared variables with υ_1 and υ_2 degrees of freedom. The second-order radar cross section $\sigma_2 N(\omega_{\mathrm{DN}})$ is calculated by the method of Lipa and Barrick (1986) from simulated wave spectra.

The radar parameters are related to the existing system. For example, the HF ocean radar system of the Okinawa Subtropical Environment Remote-Sensing Center (OSERSC) is described as follows (Hisaki et al. 2001). The radio frequency is 24.5 MHz, range resolution is 1.5 km, and the beam resolution is 7.5°. This radar system is available as 896 coherent I and Q signals at 0.5-s intervals. These signals are processed using a 256-point fast Fourier transform (FFT) after applying the Hamming window and overlapping by 50%. The degrees of freedom at one spectral point is 11 (Hisaki 1999). There are approximately 1.3 $M_{m,h} \times 11$ ($m = 1, 2$) degrees of freedom of $P_I(m)$. The value $M_{m,h}$ ($m = 1, 2$) is the number of spectral points within negative ($m = 1$) or positive ($m = 2$) Bragg echo regions, where the spectral values are greater than half of the maximum Bragg peak level (Barrick 1980). The Doppler frequency resolution is 1/128 Hz. The radar parameters for the simulation are as follows. The radio frequency is $\omega_0/(2\pi) = 24.5$ MHz, the radio wavelength is $2\pi/\tilde{k}_0 = 12.2$ m, and the Bragg frequency $\tilde{f}_B = \tilde{\omega}_B/(2\pi) = 0.506$ Hz. Because of the computer memory requirement, N_B, N_r, and K_{DT} cannot be so large, and Doppler spectra are averaged in both the frequency domain and space. The shortest distance from the radar is $\tilde{r}_{\min} = r_{\min N}/(2\tilde{k}_0) = 9$ km, and the range resolution is $\Delta\tilde{r} = \Delta r_N/(2\tilde{k}_0) = 4.5$ km. The number of beam directions is $N_B = 4$, the number of grid points per direction is $N_r = 4$, the number of radial grid points is $N_g = 16$, the number of unknowns is $N_u = 6080$ [Eq. (30)], $\psi_{B\min} = -33.75°$, and $\Delta_{\psi B} = 22.5°$. The number of quadrature points for the integral of the second-order radar cross section is $N_q = 35$. The values of $\Delta\tilde{r}$ and $\Delta_{\psi B}$ correspond to averaged Doppler spectra on nine neighboring radial grids. The normalized Doppler frequency ω_{DN} for estimating wave spectra is $\omega_{\mathrm{DlN}}(1) \leq |\omega_{\mathrm{DN}}| \leq \omega_{\mathrm{DuN}}(1)$ or $\omega_{\mathrm{DlN}}(2) \leq |\omega_{\mathrm{DN}}| \leq \omega_{\mathrm{DuN}}(2)$ at a 0.04 interval, and $K_D(i_r, j_b) \leq 60$. Second-order Doppler spectral values close to zero are not used for wave estimation. For measured Doppler spectra, $-\omega_{\mathrm{DuN}}(1) < -\omega_{\mathrm{DlN}}(1) < -\omega_{\mathrm{dlN}}(1) < \omega_{\mathrm{duN}}(1) < -\omega_{\mathrm{DuN}}(2) < -\omega_{\mathrm{DlN}}(2) < 0 < \omega_{\mathrm{DlN}}(2) < \omega_{\mathrm{DuN}}(2) < \omega_{\mathrm{dlN}}(2) < \omega_{\mathrm{duN}}(2) < \omega_{\mathrm{DlN}}(1) < \omega_{\mathrm{DuN}}(1)$.

The Doppler frequency range $[\omega_{\mathrm{DlN}}(m), \omega_{\mathrm{DuN}}(m)]$ ($m = 1, 2$) is determined from the signal and noise levels of the measured Doppler spectrum. The Doppler frequency range $[\omega_{\mathrm{DlN}}(1), \omega_{\mathrm{DuN}}(1), \omega_{\mathrm{DlN}}(2), \omega_{\mathrm{DuN}}(2)]$ is (1.08, 1.56, 0.28, 0.92) or (1.24, 1.72, 0.12, 0.76) in the present cases. In the case of the nonlinear inversion, the range of $[\omega_{\mathrm{DlN}}(m), \omega_{\mathrm{DuN}}(m)]$ ($m = 1, 2$) can be wider than the case of the linear inversion, if the second-order HF radio wave scattering theory is valid. On the other hand, in the linearization of the integral equation relating the second-order radar cross section to the ocean wave directional spectrum, a short-wave directional spectrum is replaced with the spectral form inferred from the first-order scattering (Lipa and Barrick 1986), which is valid if the values of $|\omega_{\mathrm{DlN}}(m)|$ and $|\omega_{\mathrm{DuN}}(m)|$ ($m = 1, 2$) are close to 1 [see Fig. 2 of Hisaki (1996)]. If the signal-to-noise ratio is sufficiently high, and the second-order radio wave scattering theory is likely to describe the Doppler spectrum, it is better that the Doppler frequency range $[\omega_{\mathrm{DlN}}(m), \omega_{\mathrm{DuN}}(m)]$ ($m = 1, 2$) is taken to be wide. In case K_{DT} is large compared to the computer memory requirement, Doppler spectral values should be averaged in the Doppler frequency to reduce K_{DT} and to increase υ_2.

In the present case, the value $M_{m,h}$ is 5, and the degrees of freedom of $P_I(m)$ ($m = 1, 2$) is 72. In the present case, six of nine Doppler spectra are assumed to be available, and the degrees of freedom of averaged $P_I(m)$ is $\upsilon_1 = 72 \times 6 = 432$. The degrees of freedom of averaged $P_2(\omega_{\mathrm{DN}})$ is $\upsilon_2 = 11 \times 6 = 66$.

The weights λ_{wM} ($M = 1, \ldots, 6$) in Eq. (38) are $\lambda_{w4} = 1$ and $\lambda_{w3} = (\upsilon_1/\upsilon_2)^{1/2}$. The values of other weights are also fixed, and $\lambda_{w1} = \lambda_{w6} = 10^3$, $\lambda_{w2} = 10^4$, and $\lambda_{w5} = 0.1$ here. These values are determined empirically by estimating wave spectra for various weights.

Seven cases are demonstrated. These cases are as follows.

- Case 1-A: $\tilde{u} = 10$ m/s $\theta_w = 101.25°$.
- Case 1-B: Same wind fields as case 1-A, but only one beam ($j_b = 3$) is used: the radar cross-section equations [Eqs. (2) and (3)] and the regularization constraint [Eq. (27) or (28)] are used ($\lambda_{w1} = \lambda_{w2} = \lambda_{w6} = 0$ for all j_b, and $\lambda_{w3} = \lambda_{w4} = \lambda_{w5} = 0$ for $j_b = 1, 2, 4$).
- Case 1-C: The same wind fields as in case 1-A, but the initial guess of unknowns $\mathbf{x}$ is determined only by step 1 and $M_c = 16$ (section 4c).
- Case 2-A: $\tilde{u} = 10$ m s^{-1}, $\theta_w = 0°$.
- Case 2-B: The same wind fields as in case 2-A, but the second-order radar cross sections are not used for $i_r > 2$ [$K_D(i_r, j_b) = 0$ or $\lambda_{w4} = 0$ for $i_r > 2$].
- Case 3-A: $\tilde{u} = 12.5$ m s^{-1}, $\theta_w = 75°$.
- Case 3-B: The same wind fields as in case 3-A, but only one beam ($j_b = 3$) is used (the same as in case 1-B).

In these cases, the normalized significant wave heights $H_{sN} = 4E_N^{1/2}$ are less than 4, and the second-order perturbation theory of the HF radio wave scattering from the sea surface can be applied (Lipa and Barrick 1982). The Doppler frequency range is $[\omega_{\mathrm{DlN}}$

TABLE 1. Summary of the comparison between true and estimated wave parameters. The values in parentheses are rms error ratios in step 1 (section 4c).

Case	r_h	r_t	r_w	r_θ (°)
1-A	0.046 (0.031)	0.028 (0.14)	0.047	2.32 (1.95)
1-B	0.111 (0.40)	0.050 (0.049)	0.053	178.3 (178.3)
1-C	0.104 (0.67)	0.045 (0.52)	0.085	12.28 (12.34)
2-A	0.036 (0.12)	0.026 (0.10)	0.237	0.54 (0.47)
2-B	0.063 (0.19)	0.017 (0.10)	0.278	2.02 (2.18)
3-A	0.042 (0.15)	0.021 (0.027)	0.085	5.50 (6.61)
3-B	0.138 (0.16)	0.066 (0.029)	0.061	20.76 (20.76)

(1), ω_{DuN} (1), ω_{DlN} (2), ω_{DuN} (2)] = (1.08, 1.56, 0.28, 0.92) for cases 1-A, -B, -C, and 3-A, -B; and [ω_{DlN} (1), ω_{DuN} (1), ω_{DlN} (2), ω_{DuN} (2)] = (1.24, 1.72, 0.12, 0.76) for cases 2-A, -B. In case 2-B, only the first-order scattering is available for $i_r = 3, 4$.

6. Results

The rms error ratios of wave heights, periods, and winds are calculated to assess the accuracy of wave estimation as

$$r_h = \left\{\frac{1}{N_g}\sum_{i_r=1}^{N_r}\sum_{j_b=1}^{N_B}\left[1 - \frac{H_{sN}(i_r, j_b\text{:retrieved})}{H_{sN}(i_r, j_b\text{:true})}\right]^2\right\}^{1/2}, \tag{54}$$

$$r_t = \left\{\frac{1}{N_g}\sum_{i_r=1}^{N_r}\sum_{j_b=1}^{N_B}\left[1 - \frac{T_{mN}(i_r, j_b\text{:retrieved})}{T_{mN}(i_r, j_b\text{:true})}\right]^2\right\}^{1/2}, \tag{55}$$

$$r_w = \left\{\frac{1}{N_g}\sum_{i_r=1}^{N_r}\sum_{j_b=1}^{N_B}\left[1 - \frac{u_N(i_r, j_b\text{:retrieved})}{u_N(i_r, j_b\text{:true})}\right]^2\right\}^{1/2}, \tag{56}$$

$$r_\theta = \left\{\frac{1}{N_g}\sum_{i_r=1}^{N_r}\sum_{j_b=1}^{N_B}[\theta_w(i_r, j_b\text{:retrieved}) - \theta_w(i_r, j_b\text{:true})]^2\right\}^{1/2}, \tag{57}$$

where $H_{sN} = 4E_N^{1/2}$ is the normalized significant wave height, and $T_{mN} = \Omega_N E_N^{-1}$ is the normalized mean wave period. The results are summarized in Table 1.

In addition to these cases, the case in which waves propagate onshore is also investigated. The wind speed is $\tilde{u} = 10$ m s^{-1} and the wind direction is $\theta_w = 150°$ in this case. The rms error ratios are, respectively, $r_h = 0.030$, $r_t = 0.008$, and $r_\theta = 3.84°$, which shows good agreement.

Figures 4a–d show an example of the result of wave spectrum estimation for case 1-A. The range and beam direction numbers are $(i_r, j_b) = (4, 3)$. Figure 4a shows the comparison between true and retrieved second-order Doppler spectra. The true and retrieved second-order Doppler spectra agree well except $\omega_{\mathrm{DN}} < -1.6$. In this example, the wave direction is perpendicular to the beam direction, and the second-order Doppler peak associated with the dominant wave amplitude is not clear. Figure 4b compares true and retrieved frequency spectra $\Psi_N(\omega_N)$. The agreement here is also good. The true normalized significant wave height is $H_{sN} = 1.76$, and the retrieved normalized significant wave height is $H_{sN} = 1.66$. The underestimation of wave heights for perpendicular propagation waves (e.g., Wyatt 2002) can be reduced. The rms error ratios are, respectively, $r_h = 0.046$, $r_t = 0.028$, $r_w = 0.047$, and $r_\theta = 2.32°$, which shows good agreement. Figure 4c shows the true directional distribution $D(\omega_N, \theta) = G_N(\omega_N, \theta)/\Psi_N(\omega_N)$, and Fig. 4d shows the retrieved directional distribution. The agreement is also good. For example, the directional spreads become wider at higher frequencies.

Figure 4e compares true and retrieved frequency spectra $\Psi_N(\omega_N)$ in case 1-B. The true normalized significant wave height is $H_{sN} = 1.76$, and the retrieved normalized significant wave height is $H_{sN} = 1.62$, which is somewhat smaller than that for case 1-A. The values $r_t = 0.050$ and $r_w = 0.053$ are small. The wind speed is estimated only in step 2 (section 4c), and wind speed is primarily determined in step 2 for other cases. However, the value r_θ is 178.3°, which shows that the left or right ambiguity of the wind direction to the beam direction cannot be removed. The radar-estimated wave directional distribution is also almost symmetrical to the true wave directional distribution with respect to the beam direction (Figs. 4c,f). In step 1 of the initial guess (section 4c), the wind direction and wave direction, which are determined by the Monte Carlo method, are almost symmetrical to the true wave and wind directions with respect to the beam direction. The unknown $\mathbf{x}$ is converged to the solution that minimizes the objective function $U(\mathbf{x})$ [Eq. (38)] in step 2 and in the algorithm [Eq. (39)]. However, the solution to minimize the objective function $U(\mathbf{x})$ is not determined uniquely by only the single-beam-radar information. In addition, while the directional distribution broadens with increasing frequency in Fig. 4d, the spreading does not broaden at higher frequencies in Fig. 4f.

The robustness of the nonlinear minimization algorithm [Eq. (39)] to the initial guess is investigated in case 1-C. If the initial values of wave spectra are arbitrary, the algorithm did not converge to the solution. However, even in case 1-C, $r_w = 0.104$ and the esti-

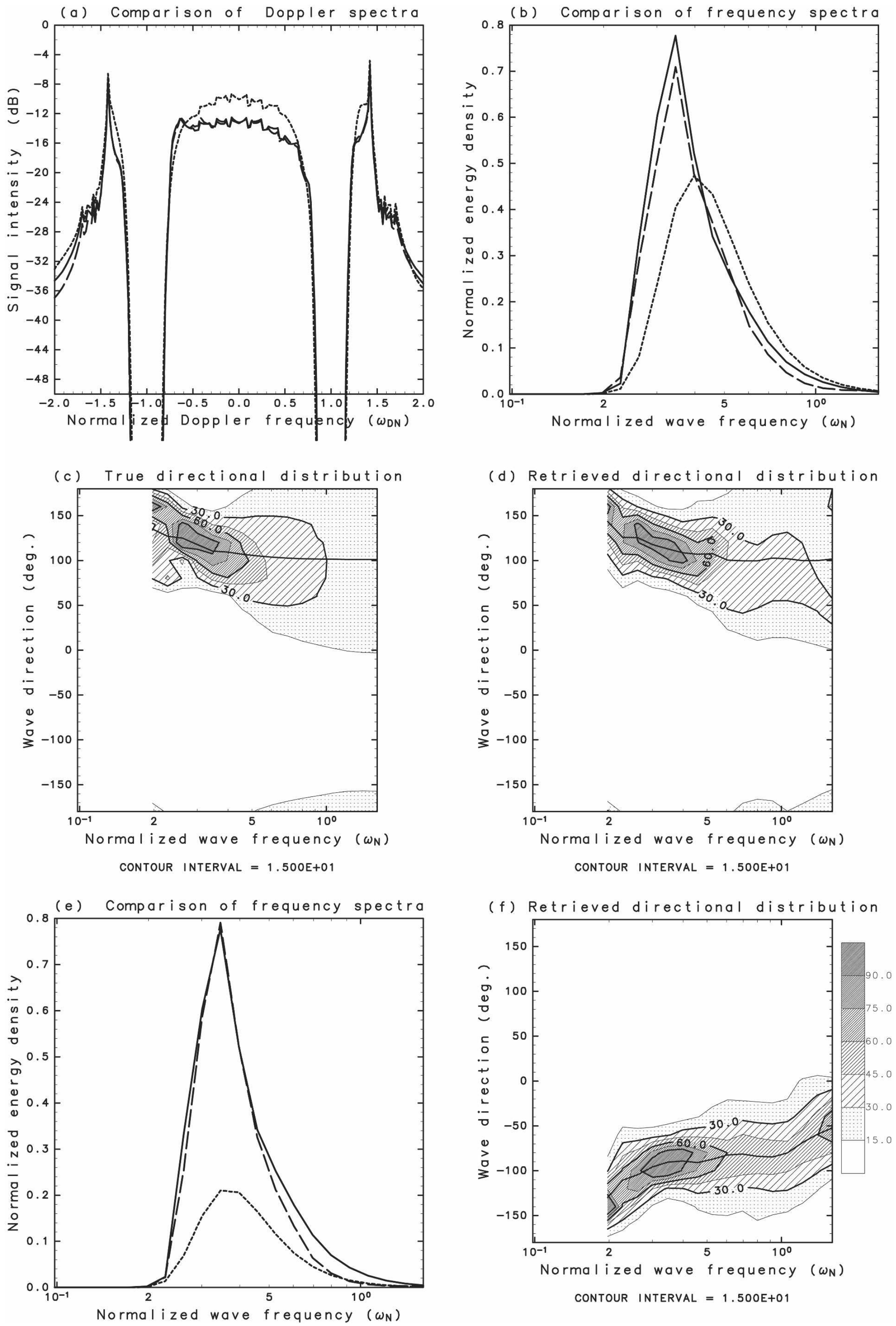

FIG. 4. Example of wave estimation for cases 1-A and 1-B and $(i_r, j_b) = (4, 3)$. (a) Second-order Doppler spectra (thick line: true; dashed line: retrieved; dotted line: initial guess in step 1) for case 1-A. (b) Frequency spectra $\Psi_N(\omega_N)$ (thick line: true; dashed line: retrieved; dotted line: initial guess in step 1), and directional distribution $D(\omega_N, \theta)$ $(\times 100) = G_N(\omega_N, \theta)/\Psi_N(\omega_N)$ for case 1-A [(c) true and (d) retrieved]. The solid lines in (c) and (d) show the mean direction as a function of the wave frequency. (e) Same as (b) but for case 1-B. (f) Same as (d) but for case 1-B.

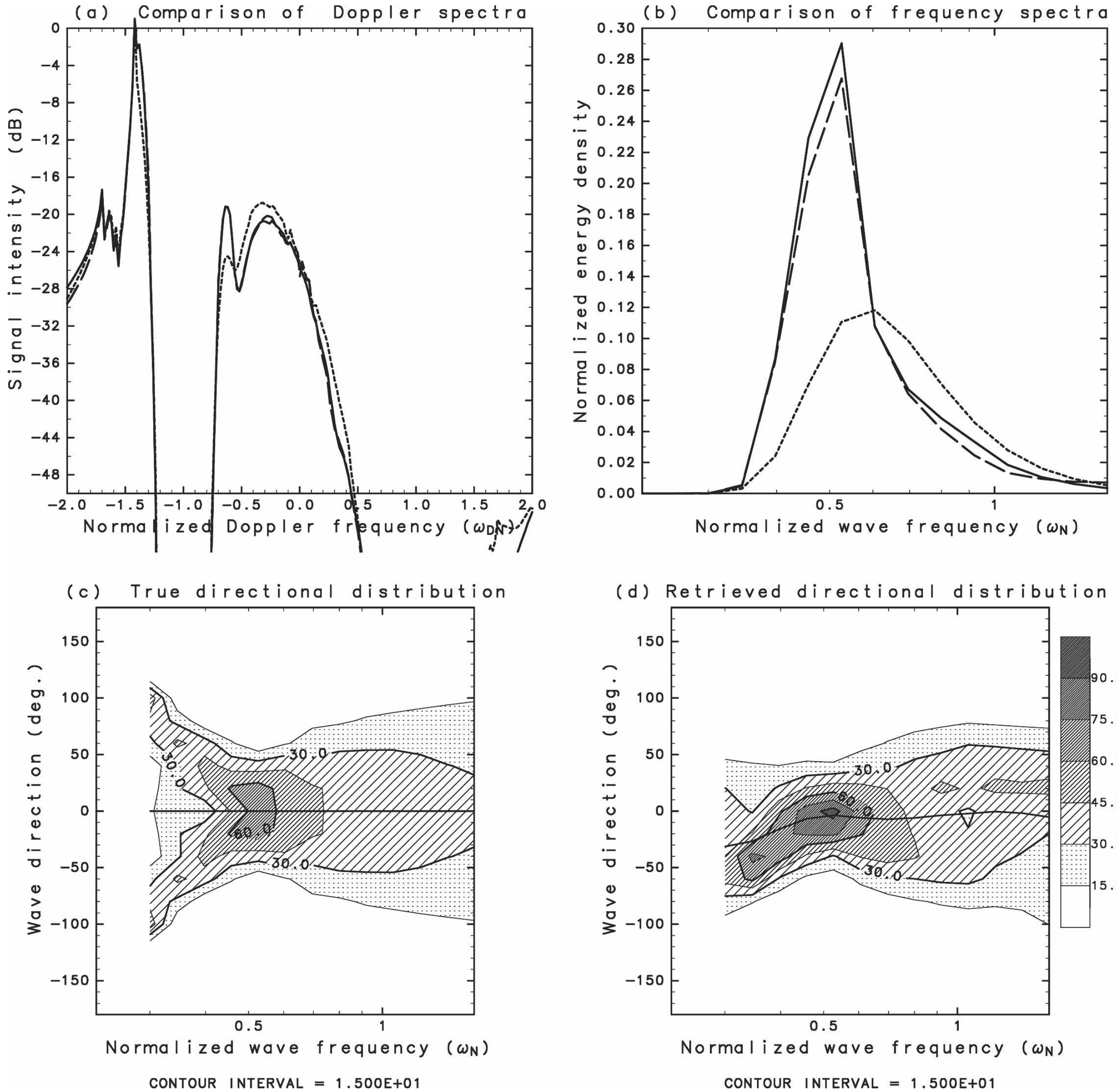

FIG. 5. Same as Fig. 4, but for case 2-A.

mated wave spectra are close to the true spectra. Thus the algorithm is robust to the initial guess.

Figure 5 shows an example of wave estimation in the fetch-limited case. The wave field is highly inhomogeneous in this case (2-A). Figure 5a compares true and retrieved second-order Doppler spectra. The wave is not fully developed, and the second-order Doppler spectral peak associated with the dominant wave is not clear. The true and retrieved second-order Doppler spectra agree well. Agreement between frequency spectra (Fig. 5b) and directional distributions is good except at lower frequencies of the directional distribution.

The rms error ratios are, respectively, $r_h = 0.036$, $r_t = 0.026$, $r_w = 0.237$, and $r_\theta = 0.54°$ (Table 1). Estimated wave heights, periods, and wind directions show good agreement with their true counterparts, although estimated wind speeds do not agree well with true wind speeds.

Figure 6 shows retrieved and true significant wave heights and periods as functions of fetch for case 2-A. The accuracies of radar-estimated wave periods for $j_b =$

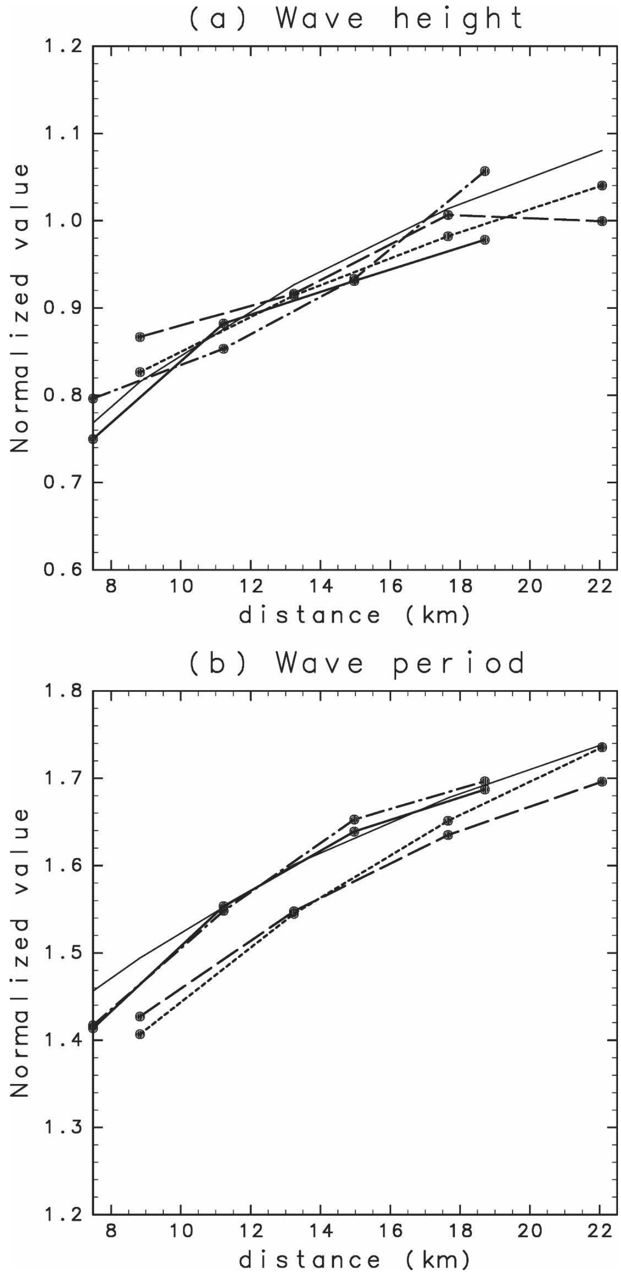

FIG. 6. Retrieved and true (a) significant wave heights and (b) periods as functions of fetch for case 2-A. Thin solid line: true value; thick solid line: $j_b = 1$; thick dashed line: $j_b = 2$; thick dotted line: $j_b = 3$; thick dashed–dotted line: $j_b = 4$.

2 and 3 are poorer than those for $j_b = 1$ and 4 because of the directional biases introduced by the single radar information when the true wave direction is almost parallel with the beam direction. As fetch increases, the true and estimated wave heights are larger and the wave periods are longer. Thus, the present method is applicable to the inhomogeneous wave field.

Figure 7 shows an example of wave estimation in case the second-order Doppler spectra at $i_r > 2$ are not used for wave estimation. The wave field is the same as that for case 2-A. The true normalized significant wave height is $H_{sN} = 1.08$, and the retrieved normalized significant wave height is $H_{sN} = 0.99$. Although the second-order Doppler spectrum is not used for wave estimation at the radial grid $(i_r, j_b) = (4, 3)$, agreements among second-order radar cross sections, wave frequency spectra, and directional distributions are good.

Figure 8 shows retrieved and true significant wave heights and periods as a function of fetch for case 2-B. In this figure, estimated wave heights are larger and wave periods are longer with increasing fetch, as in Fig. 8. The accuracies of wave height and wave period estimation for $i_r > 2$ are not as good as those in Fig. 6, but the present method is valid for wave estimation at positions where the second-order Doppler spectra are not used for wave estimation. The rms error ratios are, respectively, $r_h = 0.063$, $r_t = 0.017$, $r_w = 0.278$, and $r_\theta = 2.02°$ (Table 1). Estimations of wave heights, wave periods, and wind directions are good, especially for wave periods. The estimation of wind speeds is not good, which was also true of case 2-A. Thus, the present method can dynamically extrapolate wave spectra, even in an inhomogeneous wave field.

Figure 9 shows an example of wave estimation in case 3-A. The wind direction is 75°, but the mean wave direction at the peak wave frequency $\omega_N = 0.3$ is 98.5°, which indicates that the non–locally generated waves are more dominant than locally generated wind waves (Fig. 9c). Although the wind field is almost homogeneous, the estimated spectrum is somewhat underestimated (Fig. 9b). The true wave height is $H_{sN} = 2.35$ and the estimated wave height is $H_{sN} = 2.24$. The rms error ratios are, respectively, $r_h = 0.042$, $r_t = 0.021$, $r_w = 0.085$, and $r_\theta = 5.50°$ (Table 1), which shows good agreement. The beam direction is almost perpendicular to the wave direction. The second-order radar cross section is the smallest in the case of dominant waves propagating perpendicular to the radar for a given wave height. The second-order Doppler peaks associated with the dominant wave cannot be seen in Fig. 9a as in Fig. 4a. Therefore, the wave height is underestimated when the waves are propagating perpendicular to the radar beam. The agreement of wave directional distribution is good. For example, the frequency dependency of mean direction is reproduced in Fig. 9d. The directional spread becomes wider with increasing wave frequencies. Thus the wave spectra can be estimated in the case of seas dominated by non–locally generated waves.

Figure 9e compares true and retrieved frequency spectra $\Psi_N(\omega_N)$ for case 3-B. The radar-estimated sig-

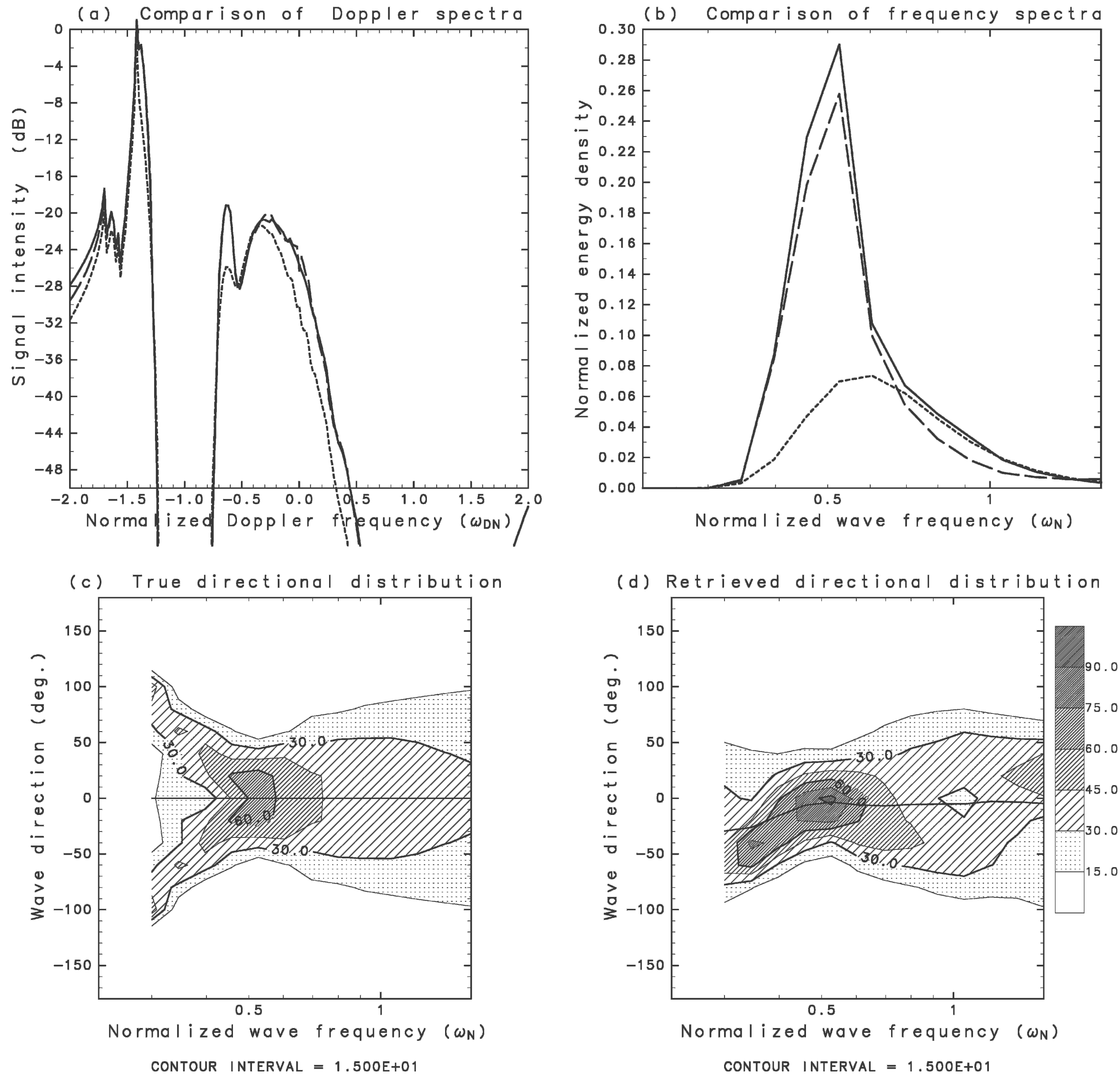

FIG. 7. Same as Fig. 5, but for case 2-B.

nificant wave height is $H_{sN} = 2.05$, which is smaller than that ($H_{sN} = 2.24$) for case 3-A as well as the true significant wave height ($H_{sN} = 2.35$). The underestimation of the wave height for the perpendicular case in Fig. 9e is more significant than that in Fig. 4e.

The rms error ratios are, respectively, $r_h = 0.138$, $r_t = 0.066$, $r_w = 0.061$, and $r_\theta = 20.76°$ (Table 1). The left or right ambiguity of the wind direction to the beam direction can be avoided. The wave direction of the initial wave spectrum determined by the Monte Carlo method (step 1 in section 4c) happened to be close to the true wave direction. The accuracy of the wave directional distribution at higher frequencies ($\omega_N > 0.6$) in Fig. 4f is poorer than that in Fig. 4d. The directional distribution does not broaden with increasing frequency in Fig. 4f.

The wave spectral values at higher frequencies are not related to the second-order scattering used in the inversion. The Doppler frequency range of the second-order scattering used in the inversion is determined from [ω_{DlN} (1), ω_{DuN} (1), ω_{DlN} (2), ω_{DuN} (2)] = (1.08, 1.56, 0.28, 0.92) (section 5a). There are wave components for $\omega_N > 0.6$ that are not related to the second-order scattering used in the inversion [see Fig. 2 of

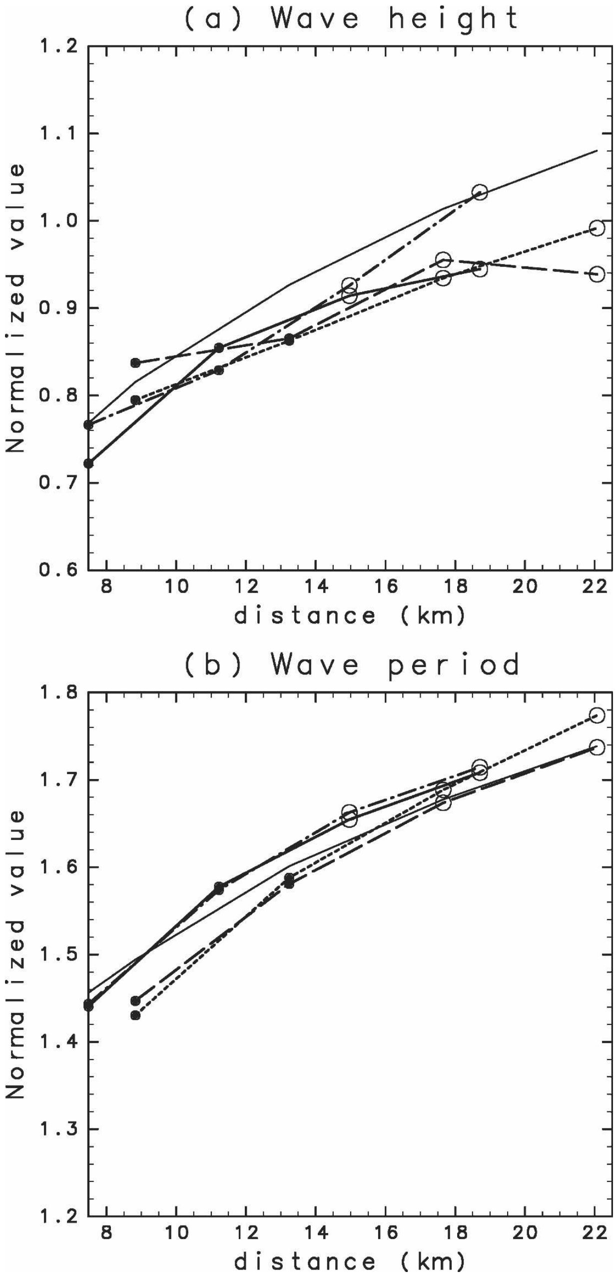

FIG. 8. Same as Fig. 6, but for case 2-B. Black circles indicate $i_r \leq 2$, and white circles indicate $i_r > 2$, where the second-order Doppler spectra are not used for wave estimation.

Hisaki (1996)]. For these wave components, spectral values are constrained only by the regularization constraint [Eq. (27) or (28)] in case 3-B. On the other hand, the spectral values at high frequencies are constrained by the energy balance equation [Eq. (9)] in case 3-A. It is possible to estimate wave directional distribution at high frequencies for case 3-A. This result shows that the parameterization of the source function is important, especially for estimating wave spectra at high frequencies.

The wind direction can be estimated from first-order scattering (e.g., Harlan and Georges 1994; Hisaki 2002) and first-order peaks that are well above the noise. Therefore, wind direction can be accurately determined. The wind speeds are primarily determined from short-wave spectral values, as explained in section 4c. High-frequency wave spectral values are sensitive to the noise of the Doppler spectrum, and thus it is difficult to estimate wind speeds accurately.

The initial Doppler and frequency spectra in step 1 are also plotted in Figs. 4, 5, 7, and 9. The comparison of wave parameters and wind directions are also shown in Table 1. The initial wave spectra are different from final estimated spectra. The values of s in Eq. (47) are not dependent on wave frequencies, which are different from final estimated directional spectra. The inversion with the wave model is effective. On the other hand, wind directions are determined primarily in step 1.

7. Conclusions

The author developed a method to estimate wave directional spectra from HF ocean radar by incorporating the energy balance equation. This method can estimate wave directional spectra with a single-array HF radar. The left or right ambiguity of the wave direction to the beam direction can be avoided without assuming a homogeneous wave field. The underestimation of wave heights in cases where the dominant wave propagates perpendicular to the beam direction can also be reduced. This method can estimate wave directional spectra in highly inhomogeneous wave fields. Furthermore, it is possible to fill gaps in wave data coverage by dynamic interpolation or extrapolation, even in a highly inhomogeneous wave field. By incorporating the wave energy balance equation, wave directional spectra can be estimated even at a position where only first-order Doppler spectra are available. In addition, the wave energy balance equation makes it possible to estimate wave directional spectra even at high frequencies, to which the second-order Doppler spectral values used for the inversion are not related. The parameterization of the source function is important, especially for estimating wave spectra at high frequencies. However, if the wave directional distribution is bimodal at high frequencies (Ewans 1998; Hwang et al. 2000; Wang and Hwang 2001), it is difficult to detect the bimodality, as discussed in section 3d. The improvement of source function parameterization is the next subject of this study. We can easily extend the present method to dual-radar systems.

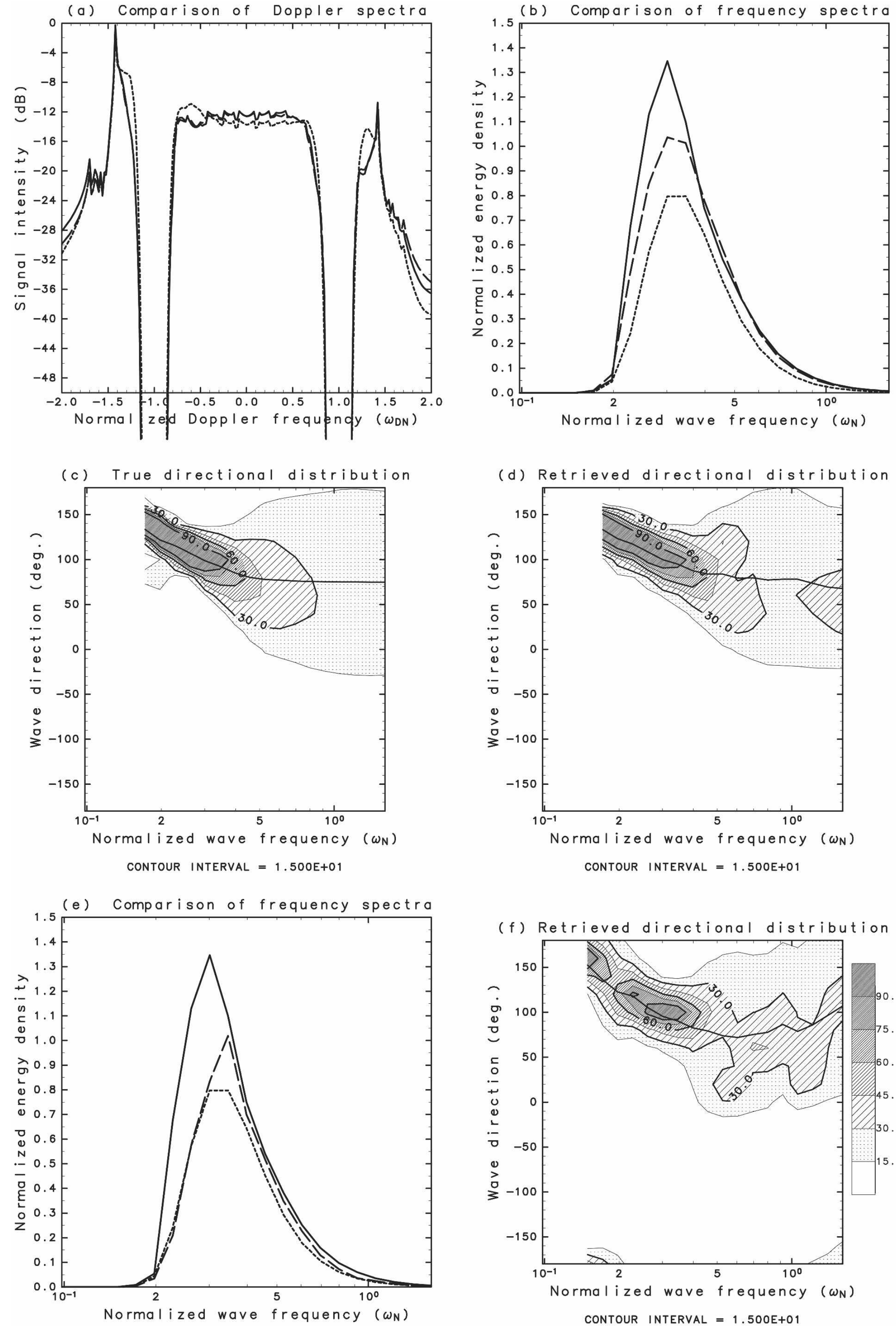

FIG. 9. Same as Fig. 4, but for cases (a)–(d) 3-A and (e) and (f) 3-B.

As shown in case 3-A, it is possible to estimate wave spectra in the case of non–locally generated waves. A swell that has propagated a long distance has a distinct spectral peak, and the second-order Doppler spectrum has significant peaks associated with the swell. Therefore, it is possible to estimate wave spectra in swell-dominant conditions, although the WAM model tends to underestimate peak wave heights in swell conditions (e.g., Bender 1996). In fact, Hisaki (2005) showed examples of wave spectrum estimation from observed Doppler spectra in swell conditions.

The present method is a single self-consistent method: The only available data are the Doppler spectra, and both winds and waves are obtained from the Doppler spectra. However, the method that would rely on the forecasted wind can also be considered. This improvement of the method can improve the accuracy of wave spectra, especially at positions where there are no second-order Doppler spectra.

In addition to the comparison of estimated wave spectra with in situ observations, a few problems must be solved. One is to investigate the validity of the present method in cases where the wave field is not stationary. Another is to develop a method to find the optimal value of weight λ_{wM} in Eq. (38). It is difficult to apply the method of Hashimoto and Tokuda (1999), because this method requires a prohibitive amount of computer memory. Furthermore, a method to estimate wind speed should be developed. These problems are the next subjects of this study.

Acknowledgments. The author acknowledges the anonymous reviewers for their insightful comments, which contributed to the improvement of the manuscript. This study was financially supported by a Grant-in-Aid for Scientific Research (C-2) from the Ministry of Education, Culture, Sports, Science, and Technology of Japan (16540403). The GFD-DENNOU Library (http://dennou.gaia.h.kyoto-u.ac.jp/arch/dcl/) was used for drawing the figures.

REFERENCES

Banner, M. L., and L. R. Young, 1994: Modeling spectral dissipation in the evolution of wind waves. Part I: Assessment of existing model performance. *J. Phys. Oceanogr.,* **24,** 1550–1571.

Barrick, D. E., 1971: Dependence of second-order Doppler sidebands in HF sea echo upon sea state. *G-AP Int. Symp. Dig.,* 194–197.

——, 1980: Accuracy of parameter extraction from sample-averaged sea-echo Doppler spectra. *IEEE Trans. Antennas Propag.,* **28,** 1–11.

Bender, L. C., 1996: Modification of the physics and numerics in a third-generation ocean wave model. *J. Atmos. Oceanic Technol.,* **13,** 726–750.

de Valk, C., A. Reniers, J. Atanga, A. Vizinho, and J. Vogelzang, 1999: Monitoring surface waves in coastal waters by integrating HF radar measurement and modelling. *Coastal Eng.,* **37,** 431–453.

Ewans, K. C., 1998: Observations of the directional spectrum of fetch-limited waves. *J. Phys. Oceanogr.,* **28,** 495–512.

Harlan, J. A., and T. M. Georges, 1994: An empirical relation between ocean-surface wind direction and the Bragg line ratio of HF radar sea echo spectra. *J. Geophys. Res.,* **99,** 7971–7978.

Hashimoto, N., and M. Tokuda, 1999: A Bayesian approach for estimation of directional wave spectra with HF radar. *Coastal Eng. J.,* **41,** 137–149.

——, L. R. Wyatt, and S. Kojima, 2003: Verification of a Bayesian method for estimating directional spectra from HF radar surface backscatter. *Coastal Eng. J.,* **45,** 255–274.

Hasselmann, K., 1962: On the non-linear energy transfer in a gravity-wave spectrum, Part 1. General theory. *J. Fluid Mech.,* **12,** 481–500.

Hasselmann, S., K. Hasselmann, J. A. Allender, and T. P. Barnet, 1985: Computations and parameterizations of the nonlinear energy transfer in a gravity wave spectrum. Part II: Parameterization of the nonlinear transfer for application in wave models. *J. Phys. Oceanogr.,* **15,** 1378–1391.

Hisaki, Y., 1996: Nonlinear inversion of the integral equation to estimate ocean wave spectra from HF radar. *Radio Sci.,* **31,** 25–39.

——, 1999: Correction of amplitudes of Bragg lines in the sea echo Doppler spectrum of an ocean radar. *J. Atmos. Oceanic Technol.,* **16,** 1416–1433.

——, 2002: Short-wave directional properties in the vicinity of atmospheric and oceanic fronts. *J. Geophys. Res.,* **107,** 3188, doi:10.1029/2001JC000912.

——, 2004: Short-wave directional distribution for first-order Bragg echoes of the HF ocean radars. *J. Atmos. Oceanic Technol.,* **21,** 105–121.

——, 2005: Ocean wave directional spectra estimation from an HF ocean radar with a single antenna array: Observation. *J. Geophys. Res.,* **110,** C11004, doi:10:1029/2005JC002881.

——, and M. Tokuda, 2001: VHF and HF sea-echo Doppler spectrum for a finite illuminated area. *Radio Sci.,* **3,** 425–440.

——, and T. Naruke, 2003: Horizontal variability of near-inertial oscillations associated with the passage of a typhoon. *J. Geophys. Res.,* **108,** 3382, doi:10.1029/2002JC001683.

——, W. Fujiie, T. Tokeshi, K. Sato, and S. Fujii, 2001: Surface current variability east of Okinawa Island obtained from remotely sensed and in-situ observational data. *J. Geophys. Res.,* **106,** 31 057–31 073.

Hwang, P. A., D. W. Wang, E. J. Walsh, W. B. Krabill, and R. N. Swift, 2000: Airborne measurements of the wavenumber spectra of ocean surface waves. Part II: Directional distribution. *J. Phys. Oceanogr.,* **30,** 2768–2787.

Komen, G. J., K. Hasselmann, and K. Hasselmann, 1984: On the existence of a fully developed wind–sea spectrum. *J. Phys. Oceanogr.,* **14,** 1271–1285.

Lipa, B. J., and D. E. Barrick, 1982: CODAR measurements of ocean surface parameters at ARSLOE—Preliminary results. *IEEE Oceans 82 Conf. Rec.,* 901–906.

——, and ——, 1986: Extraction of sea state from HF radar sea echo: Mathematical theory and modeling. *Radio Sci.,* **21,** 81–100.

Snyder, R. L., F. W. Dobson, J. A. Elliott, and R. B. Long, 1981: Array measurements of atmospheric pressure fluctuations above surface gravity waves. *J. Fluid Mech.,* **102,** 1–59.

Takeoka, H., Y. Tanaka, Y. Ohno, Y. Hisaki, A. Nadai, and H. Kuroiwa, 1995: Observation of the Kyucho in the Bungo Channel by HF radar. *J. Oceanogr.,* **51,** 699–711.

Tolman, L., 1992: Effects of numerics on the physics in a third-generation wind-wave model. *J. Phys. Oceanogr.,* **22,** 1095–1111.

WAMDI Group, 1988: The WAM model—A third generation ocean wave prediction model. *J. Phys. Oceanogr.,* **18,** 1775–1810.

Wang, D. W., and P. A. Hwang, 2001: Evolution of the bimodal directional distribution of ocean waves. *J. Phys. Oceanogr.,* **31,** 1200–1221.

Wu, J., 1980: Wind-stress coefficients over sea surface near neutral conditions—A revisit. *J. Phys. Oceanogr.,* **10,** 727–740.

Wyatt, L. R., 1990: A relaxation method for integral inversion applied to HF radar measurement of the ocean wave directional spectra. *Int. J. Remote Sens.,* **11,** 1481–1494.

——, 2002: An evaluation of wave parameters measured using a single HF radar system. *Can. J. Remote Sens.,* **28,** 205–218.

Young, I. R., L. A. Verhagen, and M. L. Banner, 1995: A note on the bimodal directional spreading of fetch-limited wind waves. *J. Geophys. Res.,* **100,** 773–778.